ADVANCED OPTICAL MATERIALS
www.advopticalmat.de

Effects of Vanadium Doping on the Optical Response and Electronic Structure of WS_2 Monolayers

*Frederico B. Sousa, Boyang Zheng, Mingzu Liu, Geovani C. Resende, Da Zhou, Marcos A. Pimenta, Mauricio Terrones, Vincent H. Crespi, and Leandro M. Malard**

2D dilute magnetic semiconductors have been recently reported in transition metal dichalcogenides doped with spin-polarized transition metal atoms, for example vanadium-doped WS_2 monolayers, which exhibit room-temperature ferromagnetic ordering. However, a broadband characterization of the electronic band structure of these doped WS_2 monolayers and its dependence on vanadium concentration is still lacking. Therefore, power-dependent photoluminescence, resonant four-wave mixing, and differential reflectance spectroscopies are performed here to study optical transitions close to the A exciton energy of vanadium-doped WS_2 monolayers at three different doping levels. Instead of a single A exciton peak, vanadium-doped samples exhibit two photoluminescence peaks associated with transitions from a donor-like level and the conduction band minima. Moreover, resonant Raman and second-harmonic generation experiments reveal a blueshift in the B exciton energy but no energy change in the C exciton after vanadium doping. Density functional theory calculations show that the band structure is sensitive to the Hubbard *U* correction for vanadium, and several scenarios are proposed to explain the two photoluminescence peaks around the A exciton energy region. This work provides the first broadband optical characterization of these 2D dilute magnetic semiconductors, shedding light on the novel and tunable electronic features of V-doped WS_2 monolayers.

1. Introduction

Tuning the electronic, optical, magnetic, and physico-chemical properties of 2D transition metal dichalcogenides (TMDs) through defect engineering provides multiple pathways for diverse applications.[1–5] For example, a dilute magnetic semiconductor (DMS)[6] can be achieved by incorporating transition metal atoms as substitutional defects in TMD monolayers.[7–12] Vanadium-doped WSe_2[10,11] and WS_2[12] samples have shown long-range ferromagnetic ordering even above room temperature, thus opening possibilities for spintronic device fabrication. However, among the significant challenges to be overcome in this field, such as gate-tunability and the enhancement of the magnetic moments,[13,14] there is a fundamental need for broadband optical and electronic structure characterization of these doped 2D semiconductors.

Here, we study pristine and V-doped WS_2 monolayer samples with three different doping levels (low, moderate, and high V doping) to explore the dependence of the optical response on the vanadium concentration near the three main excitonic energies (A, B, and C excitons), using power-dependent photoluminescence (PL), resonant Raman spectroscopy, resonant four-wave mixing (FWM) and second-harmonic generation (SHG) spectroscopies, and differential reflectance spectroscopy. Power-dependent PL, resonant FWM, and differential reflectance spectroscopies showed a splitting of the A exciton with one peak blueshifting and the other one redshifting

F. B. Sousa, G. C. Resende, M. A. Pimenta, L. M. Malard
Departamento de Física
Universidade Federal de Minas Gerais
Belo Horizonte, Minas Gerais 30123-970, Brazil
E-mail: lmalard@fisica.ufmg.br

B. Zheng, M. Liu, D. Zhou, M. Terrones, V. H. Crespi
Department of Physics
The Pennsylvania State University
University Park, PA 16802, USA

B. Zheng, V. H. Crespi
The Materials Research Institute
The Pennsylvania State University
University Park, PA 16802, USA

M. Liu, D. Zhou, M. Terrones, V. H. Crespi
Center for 2-Dimensional and Layered Materials
The Pennsylvania State University
University Park, PA 16802, USA

M. A. Pimenta
Departamento de Física
Universidade Federal de Ouro Preto
Ouro Preto, Minas Gerais 35400-000, Brazil

M. Terrones, V. H. Crespi
Department of Materials Science and Engineering
The Pennsylvania State University
University Park, PA 16802, USA

The ORCID identification number(s) for the author(s) of this article can be found under https://doi.org/10.1002/adom.202400235

DOI: 10.1002/adom.202400235

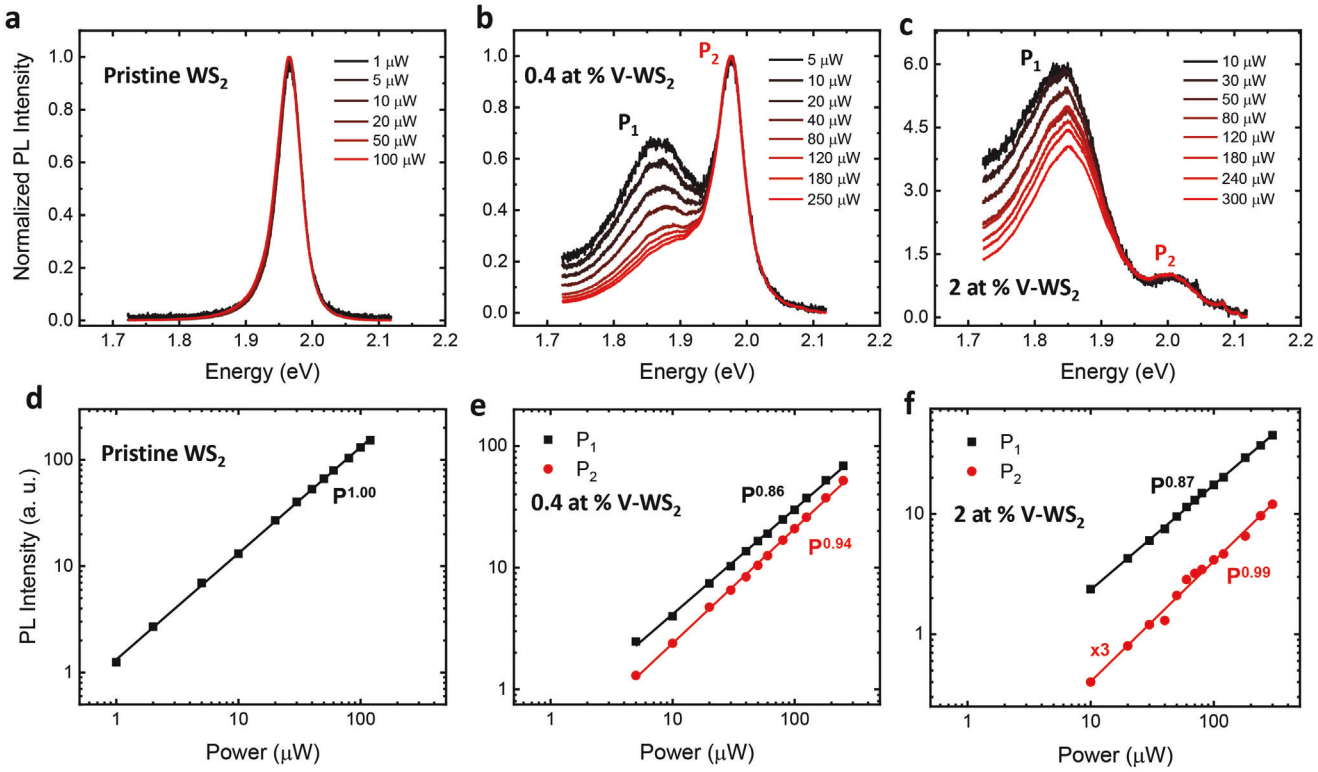

Figure 1. a–c) Normalized room temperature PL spectra for pristine (a), ≈0.4 at% (b), and ≈2.0 at% (c) vanadium doped WS_2 monolayers with different laser powers. All spectra were obtained with an excitation wavelength of 561 nm and were normalized by the higher energy peak (P_2) intensity. d–f) Power-dependent PL intensity showing a linear power dependence for the pristine WS_2 peak and V-doped WS_2 higher energy peak (P_2) and a sublinear dependence for the V-doped WS_2 lower energy peak (P_1).

under increasing vanadium doping. In addition, the sublinear power dependence of the P_1 PL peak intensity indicates an optical transition from a donor-like state. The Raman resonances show a blueshifting B exciton energy, while SHG resonant profiles show no change in the C exciton energy with increasing vanadium concentration. Density functional theory (DFT) calculations for the band structure of V-doped WS_2 with a Hubbard U correction ($U = 0$ to 5 eV) for vanadium, including transition dipole moments, were performed to elucidate the optical transitions observed in experiment. Beyond broadband optical characterization, our work also shows the potential of resonant Raman and nonlinear techniques to probe electronic features in doped 2D semiconductors.

2. Results and Discussion

2.1. Power-Dependent Photoluminescence

The pristine and V-doped WS_2 monolayers used in this work were synthesized by single-step chemical vapor deposition (CVD) as described by Zhang et al.[12] (a detailed description of the growth of the samples can be found in Methods). To confirm the presence of substitutional V atoms at W sites and to determine their concentration, high-angular annular dark-field scanning transmission electron microscopy (HAADF-STEM) imaging was performed in four distinct samples, as shown in Figure S1a–d (Supporting Information). Besides the pristine sample (Figure S1a, Supporting Information), a statistical analysis of Figure S1b–d (Supporting Information) revealed the atomic percentages (at.%) of vanadium to be ≈0.4 at.%, ≈2.0 at.%, and ≈8.0 at.%, respectively (refer to Experimental Section for a detailed description of the vanadium concentration calculation). Therefore, we were able to investigate the impact of vanadium dopants in the WS_2 monolayer on optical properties at three different doping levels: low (≈0.4 at.%), moderate (≈2.0 at.%), and high (≈8.0 at.%).

To experimentally study the electronic structure modifications in these samples due to vanadium doping, we first employed room-temperature power-dependent PL measurements with an excitation wavelength of 561 nm, as shown in **Figure 1a–c** (PL measurements for the ≈8.0 at.% sample are shown in Figure S2, Supporting Information). While the pristine sample exhibits a single PL peak at 1.96 eV related to the A exciton emission,[15,16] the doped samples display one peak in the energy range of 1.8–1.9 eV (we call P_1) and a second peak at ≈2.0 eV (P_2), similar to reported results.[17] As the doping level increases, the P_1 peak redshifts and the P_2 peak blueshifts. The PL spectra were normalized by the P_2 intensity (A exciton intensity in the case of pristine WS_2). Similar to other works,[18–20] the substitutional defects broaden the PL peak and reduce the integrated PL intensity. For comparison, the A exciton peak in the pristine sample presents a full width at half maximum (FWHM) of approximately 40 meV, while the P_1 peak exhibits a FWHM in the range of 100–150 meV for the doped monolayers. All PL spectra were fit by

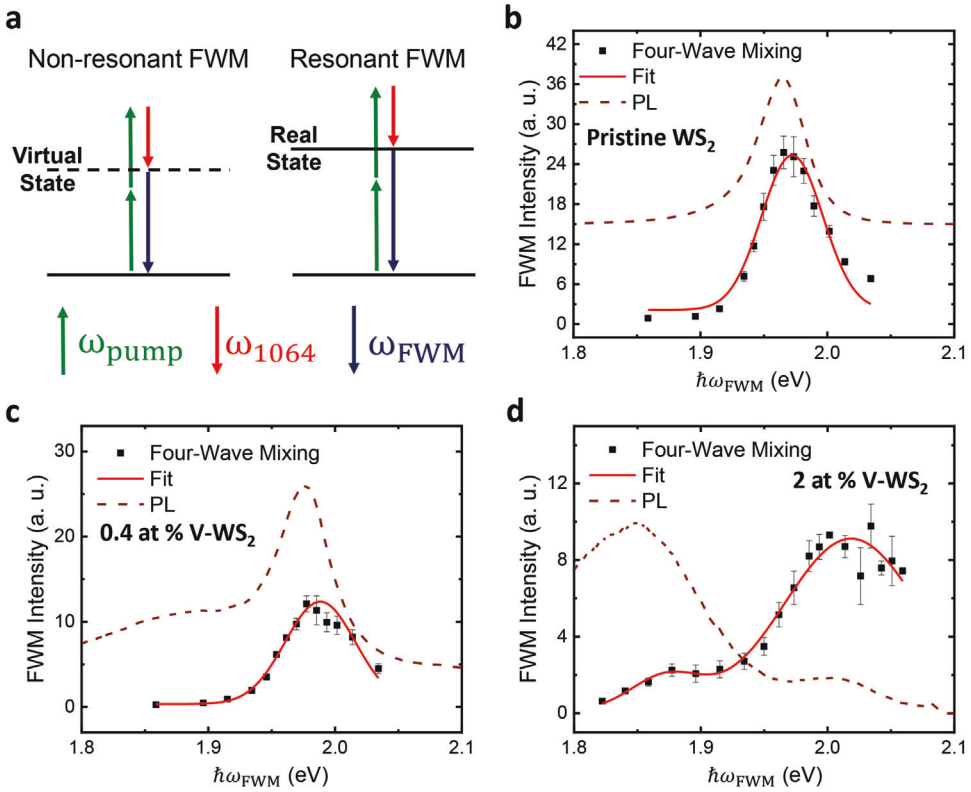

Figure 2. a) FWM energy diagrams for non-resonant and resonant conditions. The colored arrows correspond to the photons of the FWM process as described by Equation (1), and the solid (dashed) black lines represent real (virtual) states. b–d) Four-wave mixing (FWM) resonant profile (black squares) and its Gaussian fit (red line) together with the PL spectra (dashed brown line) for pristine (b), ≈0.4 at% (c), and ≈2.0 at.% (d) vanadium-doped WS_2 monolayers. The FWM resonances align with the P_2 peak for the V-doped samples. The laser powers for ω_{pump}, ω_{1064}, and PL are 5mW, 5mW, and 100μ W, respectively.

Gaussian peaks; their intensities as a function of laser power are shown in Figure 1d–f. Beside the expected linear power dependence of the A exciton peak in pristine WS_2, there is a linear (for P_2) or sublinear (for P_1) power dependence for V-doped samples. This P_2 linearity indicates[21,22] that it is associated with an exciton emission, while the sublinearity of P_1 means that it is related to a radiative recombination process from a donor or to an acceptor level. As HAADF-STEM data reveal no increase in S vacancies in the V-doped samples, similar to Ref. [17], this donor or acceptor level should be related to vanadium dopants. Although DFT calculations without Hubbard U correction show no mid-gap states,[12,23] here, we show a donor-like state near the conduction band minima when a U correction for vanadium is included, as we discuss later. Hence, the P_1 peak is presumably related to this donor-like level.

We also performed PL experiments at low temperatures (from 4 to 80 K) for ≈0.4 at.% and ≈2.0 at.% doped samples, as shown in Figure S3 (Supporting Information). While the P_2 peak dominates the ≈0.4 at.% sample's PL spectra at low temperatures, the ≈2.0 at.% doped monolayer presents both P_1 and P_2 PL peaks. In either case, we see no sign of multiple emissions in these two peaks. In addition, the PL spectra at low temperatures (as well as at room temperature) show a broader P_1 peak for the ≈2.0 at.% sample as compared to the A exciton peak from the pristine sample. This broader linewidth might be related to a shorter lifetime of the excited electrons in the V-doped monolayers, where dopants can act as scattering centers. To further investigate these electronic states, we next perform FWM and differential reflectance spectroscopy experiments.

2.2. Resonant Four-Wave Mixing

As shown by Lafeta et al.,[24] nonlinear optical techniques such as FWM can be used to determine excitonic energies. FWM is a third-order nonlinear optical process in which three photons interact in a nonlinear material to generate a fourth photon at a linear combination of the three incident photon frequencies (with coefficients ±1). Here, we measured a degenerate FWM in which two incident photons with the same variable frequency ω_{pump} (from 720 to 950 nm) interact with a third photon of a fixed frequency ω_{1064} (1064 nm) to generate a fourth photon with frequency:

$$\omega_{FWM} = 2\omega_{pump} - \omega_{1064} \quad (1)$$

Figure 2a shows the energy diagram of this degenerate FWM process for both non-resonant and resonant conditions. The wide wavelength range of the resulting ω_{FWM} (544 to 858 nm) allowed us to probe resonant responses over the energy window of the

WS_2 monolayer A exciton (600 to 680 nm). Figure 2b-d shows the FWM resonant profiles with Gaussian fits, as well as the PL spectra for three samples (pristine and doped WS_2 with ≈0.4 at.% and ≈2.0 at.% vanadium). The FWM results for the ≈8.0 at.% doped sample are not shown due to its weak intensity. The resonant behavior of the FWM data for the pristine WS_2 monolayer (Figure 2b) agrees with its single PL peak. The few-meV energy shift between the FWM resonant response and the PL peak is presumably due to a Stokes shift.[25,26] Figure 2c,d show that both the ≈0.4 and ≈2.0 at.% doped samples present a strong FWM resonant response at the energy of the P_2 peak, as well as the same Stokes shift. The ≈0.4 at.% doped sample shows no distinguishable resonance close to the lower-energy P_1 peak, while the ≈2.0 at.% doped sample shows a minor FWM resonant feature around the P_1 PL peak energy. The strong FWM resonance at the P_2 energy is in accord with reported nonlinear optical resonant response related to excitonic states at the conduction band minima in 2D TMDs.[24,27] Moreover, our results suggest that nonlinear optical resonances associated with donor-like levels are weaker than nonlinear resonances related to the conduction band.[28] Differential reflectance experiments given in Figure S4 (Supporting Information) also show that the P_2 peak dominates the absorption spectra for doped samples. As the FWM resonant response depends on the material absorption, the differential reflectance data corroborate the weaker P_1 FWM resonance.

2.3. Resonant Raman Scattering

To further characterize the electronic structure modifications in monolayer WS_2 due to vanadium doping, we performed resonant Raman spectroscopy measurements to probe the B exciton energy range. Figure S5 (Supporting Information) shows the Raman spectra of pristine and V-doped WS_2 monolayers obtained with an excitation wavelength of 521 nm. Despite a decrease in the intensity of the Raman peaks when the vanadium concentration increases to ≈2.0 at.%, there are no substantial modifications in the Raman spectra. In contrast, the Raman spectrum for the ≈8.0 at.% sample is significantly modified, reflecting alloy formation at this high doping level. In addition, Figure S6 (Supporting Information) shows Raman spectra of these pristine and V-doped WS_2 monolayers for 14 different laser lines. All spectra were normalized by the silicon peak intensity (520 cm^{-1} peak), considering its Raman cross-section[29] for each laser line. A strong dependence of the intensities of the Raman peaks on the excitation energy can be observed. This dependence, plotted as Raman excitation profile (REP), varies with the doping concentration, indicating different resonant excitation behaviors among the studied samples. The intensity of a first-order Raman mode is Ref. [30]

$$I(E_{\text{pump}}) = C\left|\sum_{m,n}\frac{\langle f|H_{e-r}|n\rangle\langle n|H_{e-ph}|m\rangle\langle m|H_{e-r}|i\rangle}{(E_{\text{exciton}}-E_{\text{pump}}+i\gamma)(E_{\text{exciton}}-E_{\text{pump}}+E_{ph}+i\gamma)}\right|^2 \quad (2)$$

where the numerator holds matrix elements for electron-radiation (H_{e-r}) and electron–phonon (H_{e-ph}) interactions between the initial (i), intermediate (m and n), and final (f) quantum states. Resonance occurs when the incident (E_{pump}) or scattered ($E_{\text{pump}} - E_{ph}$) photon energy matches the electronic transition energy (E_{exciton}). γ is a damping factor relating to the inverse lifetime of the resonant scattering process.[30]

To plot the REP, we may choose a Raman peak that has sufficient Raman intensity and to be easily identified over the measured excitation energies. **Figure 3a** shows the Raman spectrum of a pristine WS_2 monolayer obtained with 521 nm excitation. Peak positions and their Raman mode assignments have been investigated by other researchers.[31–33] Among these peaks, the 2LA(M), E_{2g}, and A_{1g} modes have the largest intensities for all the excitation energies used, as shown in Figure S7 (Supporting Information). However, 2LA(M) and E_{2g} are not ideal for plotting REP because their energies are almost degenerate, making it difficult to separate their signals, leaving A_{1g} as the best choice for plotting REP.

The A_{1g} peaks for all Raman spectra displayed in Figure S6 (Supporting Information) were fit by Lorentzian functions to extract their intensities; the resulting A_{1g} REPs are shown in Figure 3b–e. These data points were further fit by Equation (2) with the A_{1g} frequency for each sample being the phonon energy E_{ph}, and then plotted as red lines. As the pristine, ≈0.4 at.%, and ≈2.0 at.% samples present two resonant responses (one centered around 2.4 eV and another at higher energies), we have used two distinct values of E_{exciton} to fit the data. The ascertainment of the resonant energy value around 2.4 eV is not affected by the uncertainty of the value of the higher-energy resonance because of their large spectral distance. The WS_2 monolayer with ≈8.0 at.% vanadium concentration shows only one resonant feature and thus was fit to a single value of E_{exciton}. The lower (B exciton) resonance energies produced by the fits are 2.42, 2.44, 2.49, and 2.57 eV for the pristine, ≈0.4 , ≈2.0 , and ≈8.0 at.% samples, respectively. For the pristine sample, the 2.42 eV peak agrees with reported values for the WS_2 monolayer B exciton energy measured by other groups with the same[34] and different[35] techniques. Therefore, it is reasonable to assign the REP peak energy as the B exciton energy in each sample, and thus we observe a B exciton blueshift under increasing vanadium concentration. This blueshifting feature is also observed in differential reflectance measurements and the REP of the *LA* mode of those samples, as shown in Figure S4 and S8 (Supporting Information), respectively.

Resonant SHG was also used to probe the higher-energy transitions in pristine and V-doped WS_2 samples. As shown in Figure S9 (Supporting Information), the pristine sample presents a clear resonance due to the C exciton.[36,37] Furthermore, the V-doped WS_2 samples (Figure S9, Supporting Information) show similar resonance energy, indicating that vanadium doping did not substantially modify this transition. Hence, beyond the electronic characterization of the samples, the results discussed above also demonstrate an optical method to identify the vanadium doping level in WS_2 monolayers by measuring the energy splitting and intensity ratio of P_1 and P_2 PL peaks, as well as by probing the B exciton energy. To summarize these experimental results, **Figure 4** shows P_1, P_2, B exciton and C exciton energies for WS_2 monolayers with respect to their vanadium concentration for all optical techniques used in this work. In addition, Supporting Figure S10 (Supporting Information) presents the intensity ratio of P_1 and P_2 PL peaks for the pristine and V-doped samples.

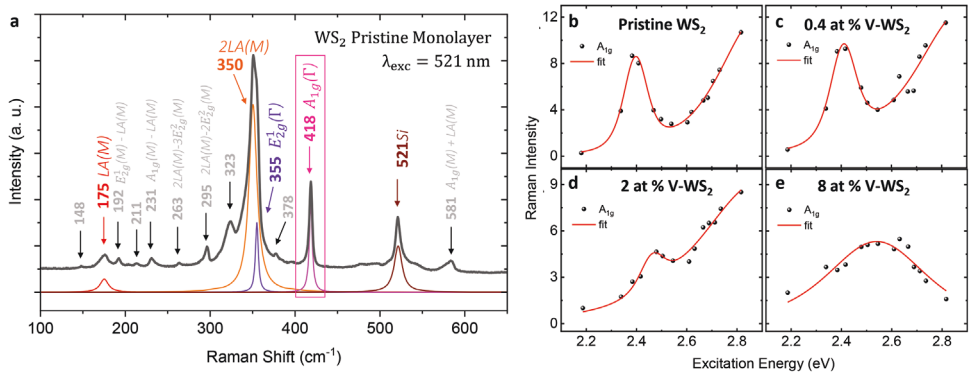

Figure 3. a) Raman spectrum of a pristine WS_2 monolayer obtained with 521 nm laser excitation. The peak positions and some of the Raman modes are assigned. The Lorentzian peak fits of selected Raman modes are shown in different colors below the spectra. b–e) Raman excitation profiles of the A_{1g} Raman mode (highlighted in pink in (a)) for the (b) pristine, (c) ≈0.4 at.%, (d) ≈2.0 at%, and (e) ≈8.0 at.% V-doped WS_2 monolayers. The solid red lines show the fits to Equation (2).

2.4. Electronic Structure Calculation

To understand the optical properties observed in experiment, we examined the band structures (Figures S11– S17, Supporting Information) of pristine and V-doped WS_2 with a Hubbard U correction ($U = 0$ to5 eV) for vanadium and calculated the transition dipole moments to identify candidate transitions, as summarized in **Figure 5**. The optical transitions in WS_2 mainly relate to the d_{x^2}/d_{xy} orbitals at the valence band maximum (VBM) and the d_{z^2} orbitals at the conduction band minima (CBM) at the K or −K valleys.[38] The defect states from the vanadium dopant mainly have the character of vanadium d_{z^2} (see **Figure 6a**), so their hybridization with the CBM is plausible. When U is small ($U \leqslant 2$ eV), the defect state in the conduction band is far from the band edge, thus it does not hybridize well with the CBM. However, the defect state still shows a non-negligible optical coupling to the valence bands at the K valley. In this case ($U \leqslant 2$ eV), the A and B excitons can be easily identified. We find a valley degeneracy breaking of ≈0.02 to ≈0.1 eV as U increases. If U further increases, the defect state in the conduction band drops in energy and hybridizes with the spin-up CBM (i.e., the same spin as the defect state). The resulting hybridized states both show large optical transition matrix elements with the d_{x^2}/d_{xy} valence bands. When $U \geqslant 3$ eV, we cannot identify the A exciton at the K valley or the B exciton at the −K valley, so we tentatively call them "upper" and "lower" spin-up transitions; we will discuss these later. This hybridization explains why the spin-up transitions are sensitive to the value of U. On the other hand, the spin-down defect states are far from the CBM and consequently do not hybridize with it; thus the spin-down transitions are insensitive to the value of U.

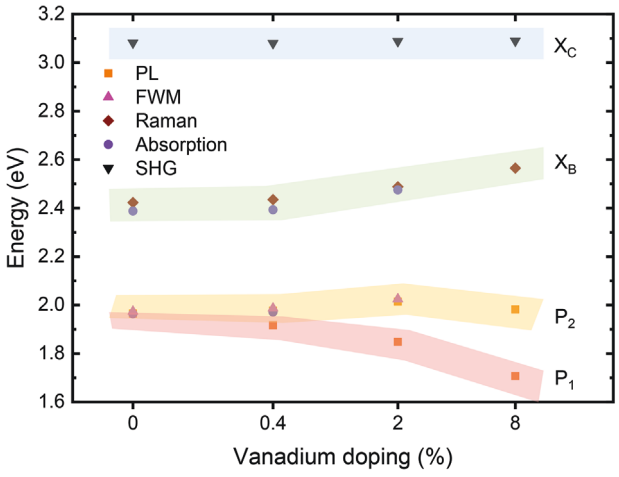

Figure 4. Summary of P_1, P_2, B exciton (X_B), and C exciton (X_C) energies for WS_2 monolayers with respect to their vanadium doping concentration measured by PL, resonant FWM, resonant Raman, absorption (differential reflectance), and resonant SHG measurements. The shadowed areas are a guide to the eyes.

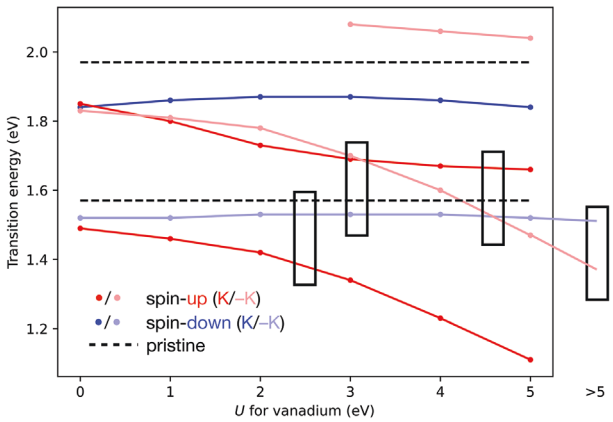

Figure 5. Transition energies with largest transition dipole moments in V-doped WS_2 (1 vanadium in a 5 × 5 supercell). The dashed line shows the calculated A, B exciton energies in pristine WS_2. The extension to $U >$ 5 eV is drawn schematically following the trend from the plot. Valley degeneracy breaking is non-negligible even without a Hubbard U correction for vanadium. The band structure and consequently the optical properties are sensitive to the value of U. As U increases, transitions associated with spin-up states redshift, while those related to spin-down states are relatively insensitive to the Hubbard U. Rectangles highlight four possible scenarios to explain the ≈0.13 eV energy difference between the P_1 and P_2 peaks.

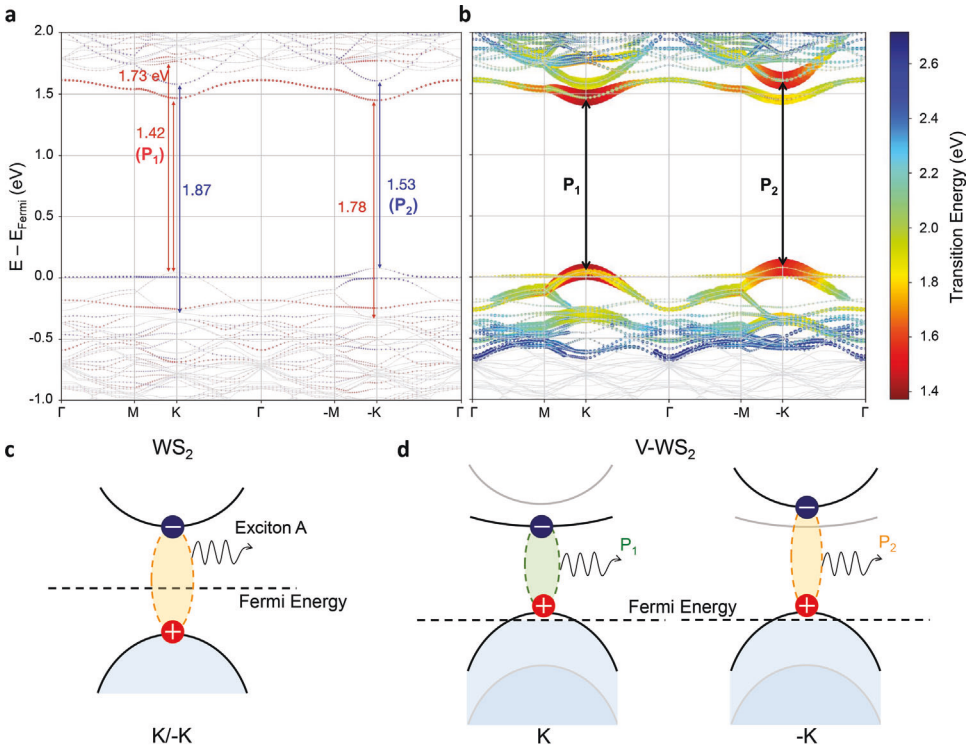

Figure 6. a) Band structure of V-doped WS_2 with $U = 2.0$ eV for vanadium. For each state, a circle is plotted with size proportional to the projection onto the vanadium d_{z^2} orbital and color indicating the spin (red=up, blue=down). The vanadium defect state in the conduction band, mainly with d_{z^2} character, has spin-up and hybridizes with the spin-up conduction band minima. The spin-down defect states remain far away from the conduction band edge. b) Band structure and transition dipole moments of V-doped WS_2 with $U = 2.0$ eV for vanadium. The energies of transitions at K with the largest transition dipole moments are 1.42;1.73;1.87eV. The energies of transitions at −K with the largest transition dipole moments are 1.53;1.78 eV. These two panels (a,b) also serve as a semi-quantitative representation of the $U \approx 2.5$ eV scenario where P_1 transition would be from a donor-like state. c,d) Schematic illustration of band structure and optical transitions for the A exciton and the P_1/P_2 in the $U \approx 2.5$ eV scenario. The pristine sample presents its degenerate A exciton recombination at K and −K valleys (c). V-doped WS_2 displays valley degeneracy breaking (d), where P_1 is from a donor-like level while P_2 is from one of the dispersive conduction band minima. The black bands are associated with P_1 or P_2 optical transitions, while the gray bands are not related to them.

Identifying the origin of the experimental peaks is not straightforward due to the sensitivity of the band structure to the value of U, in addition to the underestimation of optical transition energies in DFT at the PBE level.[39] We therefore concentrate on the ≈0.13 eV splitting of P_1 and P_2 around the A exciton energy region in Figure 1 and find four possible scenarios with U of ≈2.5; ≈3; ≈4.5; >5 eV, as highlighted by the black rectangles in Figure 5. Although there may be more than two lines in each rectangle, there are only two energies. We discuss these two energies as candidate origins for P_1 and P_2, meaning the P_1 or P_2 features may arise from more than one transition. In the $U \approx 2.5$ eV scenario, the P_1–P_2 energy difference is from the valley degeneracy breaking of the A exciton. This scenario can be semi-quantitatively represented by the $U = 2.0$ eV case (Figure 6a; S14, Supporting Information), in which the hybridization between the vanadium defect state and the spin-up CBM results in the P_1 peak transitioning from a donor-like level. In the $U \approx 3$ eV scenario (Figure S15, Supporting Information), P_1 is the A exciton at −K and P_2 could be from two transitions, namely the upper spin-up transition at K and the lower spin-up transition at −K, since their energies coincide. In the $U \approx 4.5$ eV scenario, as semi-quantitatively represented in Figure S16 (Supporting Information), the A exciton and the lower transition energies at −K have similar energies, so they both could be the P_1 peak, while the upper spin-up transition at K could be the P_2 peak. In the $U > 5$ eV scenario, as semi-quantitatively represented in Figure S17 (Supporting Information), P_1 is the lower spin-up transition and P_2 is the A exciton at −K.

Among these scenarios, $U \approx 3$; ≈4.5 eV can qualitatively explain the blueshift of the P_2 peak relative to the pristine A exciton. In the $U \approx 3$; ≈4.5; >5 eV scenarios, the high energy of the upper spin-up transition at −K (light red in Figure 5) could qualitatively explain the blueshift of the B exciton. In the $U \approx 2.5$; >5 eV scenarios, P_1 is associated with a donor-like or mid-gap state, while P_2 is associated with the dispersive band edges, which can explain the sublinear and linear behaviors of P_1 and P_2 in the power-dependent PL, respectively. Considering that in the $U \approx 2.5$ eV scenario, the P_1 and P_2 peaks are from the two transitions with the largest transition dipole moments, this scenario might be the best model identifiable at this level of theory. Although none of these scenarios can fully explain all of the optical responses observed in the experiments, they provide relevant insights into the electronic structure modifications introduced by the presence of vanadium in the WS_2 monolayer as well as its dependence on

the Hubbard *U* correction. Further investigation, for example, a more accurate calculation in the *GW*-BSE approach,[40] is needed to further elucidate the origins of these splittings/shifts in exciton energies.

3. Conclusion

In summary, we studied the dependence on vanadium doping of the electronic band structure and optical transitions in WS_2 monolayers using several optical techniques. Power-dependent PL measurements showed that the A exciton PL peak of the pristine WS_2 monolayer splits into two PL peaks after vanadium doping—one (P_1) redshifted and another (P_2) blueshifted relative to the pristine A exciton. The sublinear (linear) power dependence of P_1 (P_2) indicates that P_1 (P_2) should be related to a transition from a donor-like (CBM) state. Moreover, FWM experiments showed a strong resonance at the P_2 energy and a minor resonance at the P_1 energy, revealing a weaker nonlinear optical response associated with donor-like levels. Resonant Raman spectroscopy revealed a blueshift in the B exciton energy under increasing vanadium doping, while the SHG resonant profile revealed no modifications in the C exciton energy. First-principles calculations showed a valley degeneracy breaking after vanadium doping and a strong dependence of the band structure on the Hubbard *U* parameter for vanadium, providing relevant insights to understand the experimental data. Our work presents an optical method to help identify the vanadium doping level in WS_2 monolayers by measuring P_1, P_2, and B exciton energies, highlighting the potential of broadband optical characterization to study the impact of defects in 2D materials.

4. Experimental Section

Sample Preparation: In the liquid-assisted CVD method used to synthesize monolayer V-doped WS_2 flakes, ammonium metatungstate hydrate ($(NH_4)_6H_2W_{12}O_{40}\cdot xH_2O$) and sodium cholate hydrate ($C_{24}H_{39}NaO_5\cdot xH_2O$) powders were first mixed and dissolved in DI water to form the W precursor solution. A vanadyl sulfate ($VO[SO_4]$) powder was separately dissolved in DI water to form the V precursor solution. The two solutions were mixed and spin-coated onto SiO_2/Si substrates, and the as-treated substrates were placed in a quartz tube as the reaction chamber. A sulfur powder was placed upstream in the quartz tube, and with ultrahigh purity Ar carrier gas streaming, the quartz tube was placed in a furnace and heated to 825 °C for 15 min for the precursors to react. After the reaction, the furnace was naturally cooled to room temperature with Ar protection. Different dopant concentrations were realized by tuning the volume ratio between the W and V precursor solutions.

Doping Concentration Calculation: The dopant concentration from the STEM images by identifying the defect type at each lattice site of tungsten from the intensity and calculating the ratio between the number of V dopants and the number of tungsten sites in the FOV, which was interpreted as the atomic dopant concentration. This kind of calibration had been performed on each of the previously studied materials (see Refs. [11,12,17,41]), and the experiments were conducted only once for each precursor composition utilized in the synthesis. Therefore, the dopant concentration values should be regarded as estimates and indicators of the degree of electronic structure modification.

Spectroscopy Measurements: The FWM and SHG measurements were performed with a picosecond OPO laser (*APE* Picoemerald) with a pump power of 5 mW for both ω_{pump} and ω_{1064} for the FMW and 3 mW for the SHG. The power-dependent PL measurements were performed using a 561 nm CW diode laser. The laser beam was focused on the sample by a 40× objective with numerical aperture N.A. = 0.95. The backscattered signal was collected by the same objective and directed to the spectrometer (*Andor* Shamrock 303i) equipped with a sensitive CCD camera (*Andor* IDUS DU401A-BV). Different filters were used to reject laser light from the spectrometer: a 750 nm or an 842 nm short-pass filter for SHG and FWM and a 561 nm long-pass filter for PL measurements. Differential reflectance measurements were performed with a white light source focused on the sample by the same objective and directed to the same spectrometer.

Resonant Raman spectroscopy measurements were performed on a HORIBA *Jobin Yvon* T64000 triple-monochromator spectrometer equipped with a CCD detector and using an 1800 gmm^{-1} diffraction grating. The samples were excited by an Ar-Kr laser to cover excitation energies from 2.18 to 2.81 eV and with an incident power of 0.6 mW. A 100× objective with numerical aperture N.A. = 0.9 was used to focus the laser beam and collect the backscattered signal.

We carried out these spectroscopy measurements at distinct regions on the pristine and V-doped WS_2 monolayers and obtained a reasonable uniformity in the optical response, in contrast to non-uniformities reported in other doped TMD samples.[17,20,42]

Calculations: Density functional theory (DFT) was carried out by VASP[43–46] at the PBE level[47] with a cutoff energy of 500 eV and a 5 × 5 × 1 Monkhorst-Pack mesh.[48] The lattice constant for the supercell (1 vanadium doped in 5 × 5 WS_2) was kept five times the lattice constant of primitive WS_2 (5 × 3.188Å = 15.94Å), assuming that the low doping level would have little effect on the lattice constant. The convergence criteria for electronic self-consistency and force relaxation are 1e-7 eV and 0.01 $eVÅ^{-1}$ on all atoms. Spin-orbit coupling was included after the relaxation process for electronic structure calculations. The rotationally invariant DFT+*U* method[49] was used for the Hubbard *U* correction. Transition dipole moments were calculated with the code `VaspBandUnfolding`.[50]

Supporting Information

Supporting Information is available from the Wiley Online Library or from the author.

Acknowledgements

F.B.S. and B.Z. contributed equally to this paper as regards experimental and computational aspects, respectively. F.B.S, G.C.R, M.A.P., and L.M.M acknowledged financial support from CNPq, CAPES, FAPEMIG, FINEP, Brazilian Institute of Science and Technology (INCT) in Carbon Nanomaterials and Rede Mineira de Materiais 2D (FAPEMIG). B.Z. and V.H.C. acknowledged support from the 2DCC-MIP, which was funded by NSF cooperative agreement DMR-2039351. M.T. and D.Z. also thank AFOSR for financial support (FA9550-23-1-0447). The authors also acknowledged Prof. Marcio D. Teodoro and the GNS multiuser laboratory from the Physics Department at UFSCar for low temperature PL experiments.

Conflict of Interest

The authors declare no conflict of interest.

Data Availability Statement

The data that support the findings of this study are available from the corresponding author upon reasonable request.

Keywords

2D materials, dilute magnetic semiconductor, nonlinear optics, optics, transition metal dichalcogenides, tungsten disulfide

Received: January 25, 2024
Revised: April 8, 2024
Published online: May 3, 2024

[1] Z. Lin, B. R. Carvalho, E. Kahn, R. Lv, R. Rao, H. Terrones, M. A. Pimenta, M. Terrones, *2D Mater.* **2016**, *3*, 22002.
[2] J. Hong, C. Jin, J. Yuan, Z. Zhang, *Adv. Mater.* **2017**, *29*, 1606434.
[3] S. Wang, A. Robertson, J. H. Warner, *Chem. Soc. Rev.* **2018**, *47*, 6764.
[4] Q. Liang, Q. Zhang, X. Zhao, M. Liu, A. T. S. Wee, *ACS Nano* **2021**, *15*, 2165.
[5] S. Ippolito, P. Samorì, *Small Sci.* **2022**, *2*, 2100122.
[6] T. Dietl, H. Ohno, *Rev. Mod. Phys.* **2014**, *86*, 187.
[7] A. Ramasubramaniam, D. Naveh, *Phys. Rev. B* **2013**, *87*, 195201.
[8] Y. Wang, S. Li, J. Yi, *Sci. Rep.* **2016**, *6*, 24153.
[9] M. Habib, Z. Muhammad, R. Khan, C. Wu, Z. ur Rehman, Y. Zhou, H. Liu, L. Song, *Nanotechnology* **2018**, *29*, 115701.
[10] S. J. Yun, D. L. Duong, D. M. Ha, K. Singh, T. L. Phan, W. Choi, Y.-M. Kim, Y. H. Lee, *Adv. Sci.* **2020**, *7*, 1903076.
[11] Y. T. H. Pham, M. Liu, V. O. Jimenez, Z. Yu, V. Kalappattil, F. Zhang, K. Wang, T. Williams, M. Terrones, M.-H. Phan, *Adv. Mater.* **2020**, *32*, 2003607.
[12] F. Zhang, B. Zheng, A. Sebastian, D. H. Olson, M. Liu, K. Fujisawa, Y. T. H. Pham, V. O. Jimenez, V. Kalappattil, L. Miao, T. Zhang, R. Pendurthi, Y. Lei, A. L. Elías, Y. Wang, N. Alem, P. E. Hopkins, S. Das, V. H. Crespi, M.-H. Phan, M. Terrones, *Adv. Sci.* **2020**, *7*, 2001174.
[13] Y. H. Lee, *Science* **2023**, *382*, eadl0823.
[14] V. Ortiz Jimenez, Y. T. H. Pham, D. Zhou, M. Liu, F. A. Nugera, V. Kalappattil, T. Eggers, K. Hoang, D. L. Duong, M. Terrones, H. Rodriguez Gutiérrez, M.-H. Phan, *Adv. Sci.* **2023**, *n/a*, 2304792.
[15] H. Zeng, G.-B. Liu, J. Dai, Y. Yan, B. Zhu, R. He, L. Xie, S. Xu, X. Chen, W. Yao, X. Cui, *Sci. Rep.* **2013**, *3*, 1608.
[16] A. McCreary, A. Berkdemir, J. Wang, M. A. Nguyen, A. L. Elías, N. Perea-López, K. Fujisawa, B. Kabius, V. Carozo, D. A. Cullen, T. E. Mallouk, J. Zhu, M. Terrones, *J. Mater. Res.* **2016**, *31*, 931.
[17] T. Zhang, M. Liu, K. Fujisawa, M. Lucking, K. Beach, F. Zhang, M. Shanmugasundaram, A. Krayev, W. Murray, Y. Lei, Z. Yu, D. Sanchez, Z. Liu, H. Terrones, A. L. Elías, M. Terrones, *Small* **2023**, *19*, 2205800.
[18] F. Zhang, Y. Lu, D. S. Schulman, T. Zhang, K. Fujisawa, Z. Lin, Y. Lei, A. L. Elias, S. Das, S. B. Sinnott, M. Terrones, *Sci. Adv.* **2019**, *5*, eaav5003.
[19] S. Li, J. Hong, B. Gao, Y.-C. Lin, H. E. Lim, X. Lu, J. Wu, S. Liu, Y. Tateyama, Y. Sakuma, K. Tsukagoshi, K. Suenaga, T. Taniguchi, *Adv. Sci.* **2021**, *8*, 2004438.
[20] B. L. T. Rosa, K. Fujisawa, J. C. C. Santos, T. Zhang, M. J. S. Matos, F. B. Sousa, T. C. Barbosa, L. Lafeta, S. L. L. M. Ramos, B. R. Carvalho, H. Chacham, B. R. A. Neves, M. Terrones, L. M. Malard, *Phys. Rev. B* **2022**, *106*, 115301.
[21] T. Schmidt, K. Lischka, W. Zulehner, *Phys. Rev. B* **1992**, *45*, 8989.
[22] C. Spindler, T. Galvani, L. Wirtz, G. Rey, S. Siebentritt, *J. Appl. Phys.* **2019**, *126*, 175703.
[23] B. Schuler, J.-H. Lee, C. Kastl, K. A. Cochrane, C. T. Chen, S. Refaely-Abramson, S. Yuan, E. van Veen, R. Roldán, N. J. Borys, R. J. Koch, S. Aloni, A. M. Schwartzberg, D. F. Ogletree, J. B. Neaton, A. Weber-Bargioni, *ACS Nano* **2019**, *13*, 10520.
[24] L. Lafeta, A. Corradi, T. Zhang, E. Kahn, I. Bilgin, B. R. Carvalho, S. Kar, M. Terrones, L. M. Malard, *2D Mater.* **2021**, *8*, 35010.
[25] W. Zhao, Z. Ghorannevis, L. Chu, M. Toh, C. Kloc, P.-H. Tan, G. Eda, *ACS Nano* **2013**, *7*, 791.
[26] P. Fan, B. Zheng, X. Sun, W. Zheng, Z. Xu, C. Ge, Y. Liu, X. Zhuang, D. Li, X. Wang, X. Zhu, Y. Jiang, A. Pan, *J. Phys. Chem. Lett.* **2019**, *10*, 3763.
[27] S. Shree, D. Lagarde, L. Lombez, C. Robert, A. Balocchi, K. Watanabe, T. Taniguchi, X. Marie, I. C. Gerber, M. M. Glazov, L. E. Golub, B. Urbaszek, I. Paradisanos, *Nat. Commun.* **2021**, *12*, 6894.
[28] J. Ruan, Y.-H. Chan, S. G. Louie, arXiv preprint arXiv:2310.09674 **2023**.
[29] P. Lautenschlager, M. Garriga, L. Vina, M. Cardona, *Phys. Rev. B* **1987**, *36*, 4821.
[30] A. Jorio, M. S. Dresselhaus, R. Saito, G. Dresselhaus, in *Raman Spectroscopy in Graphene Related Systems*, Wiley, New York **2011**, pp. 73–101.
[31] A. Berkdemir, H. R. Gutiérrez, A. R. Botello-Méndez, N. Perea-López, A. L. Elías, C.-I. Chia, B. Wang, V. H. Crespi, F. López-Urías, J.-C. Charlier, H. Terrones, M. Terrones, *Sci. Rep.* **2013**, *3*, 1755.
[32] M. Thripuranthaka, R. V. Kashid, C. Sekhar Rout, D. J. Late, *Appl. Phys. Lett.* **2014**, *104*, 81911.
[33] K. M. McCreary, A. T. Hanbicki, S. Singh, R. K. Kawakami, G. G. Jernigan, M. Ishigami, A. Ng, T. H. Brintlinger, R. M. Stroud, B. T. Jonker, *Sci. Rep.* **2016**, *6*, 35154.
[34] E. del Corro, A. Botello-Méndez, Y. Gillet, A. L. Elias, H. Terrones, S. Feng, C. Fantini, D. Rhodes, N. Pradhan, L. Balicas, X. Gonze, J.-C. Charlier, M. Terrones, M. A. Pimenta, *Nano Lett.* **2016**, *16*, 2363.
[35] B. Zhu, X. Chen, X. Cui, *Sci. Rep.* **2015**, *5*, 9218.
[36] L. M. Malard, T. V. Alencar, A. P. M. Barboza, K. F. Mak, A. M. de Paula, *Phys. Rev. B* **2013**, *87*, 201401.
[37] F. B. Sousa, L. Lafeta, A. R. Cadore, P. K. Sahoo, L. M. Malard, *2D Mater.* **2021**, *8*, 35051.
[38] G.-B. Liu, W.-Y. Shan, Y. Yao, W. Yao, D. Xiao, *Phys. Rev. B* **2013**, *88*, 085433.
[39] J. M. Crowley, J. Tahir-Kheli, W. A. I. Goddard, *J. Phys. Chem. Lett.* **2016**, *7*, 1198.
[40] M. Marsili, A. Molina-Sánchez, M. Palummo, D. Sangalli, A. Marini, *Phys. Rev. B* **2021**, *103*, 155152.
[41] T. Zhang, K. Fujisawa, F. Zhang, M. Liu, M. C. Lucking, R. N. Gontijo, Y. Lei, H. Liu, K. Crust, T. Granzier-Nakajima, H. Terrones, A. L. Elías, M. Terrones, *ACS Nano* **2020**, *14*, 4326.
[42] J. Zou, Z. Cai, Y. Lai, J. Tan, R. Zhang, S. Feng, G. Wang, J. Lin, B. Liu, H.-M. Cheng, *ACS Nano* **2021**, *15*, 7340.
[43] G. Kresse, J. Furthmüller, *Comput. Mater. Sci.* **1996**, *6*, 15.
[44] G. Kresse, J. Furthmüller, *Phys. Rev. B* **1996**, *54*, 11169.
[45] G. Kresse, J. Hafner, *Phys. Rev. B* **1993**, *47*, 558.
[46] G. Kresse, D. Joubert, *Phys. Rev. B* **1999**, *59*, 1758.
[47] J. P. Perdew, K. Burke, M. Ernzerhof, *Phys. Rev. Lett.* **1996**, *77*, 3865.
[48] H. J. Monkhorst, J. D. Pack, *Phys. Rev. B* **1976**, *13*, 5188.
[49] A. I. Liechtenstein, V. I. Anisimov, J. Zaanen, *Phys. Rev. B* **1995**, *52*, R5467.
[50] Q. Zheng, VaspBandUnfolding, https://github.com/QijingZheng/VaspBandUnfolding (accessed: 2023).

